Short-term variability of atmospheric helium revealed through a cryo-enrichment method

Benjamin Birner[1], Eric Morgan[1], and Ralph F. Keeling[1]
[1]Scripps Institution of Oceanography, University of California San Diego, La Jolla, CA 92037, USA

Correspondence to: Benjamin Birner (bbirner@ucsd.edu)

Abstract. Tropospheric helium variations are tightly linked to CO_2 due to the co-emission of He and CO_2 from natural gas burning. Recently Birner et al. (2022) showed that the global consumption of natural gas has measurably increased the He content of the atmosphere. Like CO_2, He is also predicted to exhibit complex spatial and temporal variability on shorter time scales, but measurements of these short-term variations are lacking. Here we present the development of an improved gas delivery and purification system for the semi-continuous mass spectrometric measurement of the atmospheric He-to-nitrogen ratio (He/N_2). The method replaces the chemical getter used previously by Birner et al. (2021, 2022) to preconcentrate He in an air stream with a cryogenic trap which can be more simply regenerated by heating and which improves the precision of the measurement to 22 per meg (i.e., 0.022 per mille) in 10 minutes (1σ). Using this "cryo-enrichment" method, we measured the He/N_2 ratios in ambient air at La Jolla (California, USA) over 5 weeks in 2022. During this period, He/N_2 was strongly correlated with atmospheric CO_2 concentrations, as expected from anthropogenic emissions, with a diurnal cycle of 450-500 per meg (max-min) caused by the sea/land breeze pattern of local winds, which modulates the influence of local pollution sources.

Short non-technical summary. Atmospheric variations of helium (He) and CO_2 are strongly linked due to the co-released of both gases from natural gas burning. This implies atmospheric He measurements may be a potentially powerful tool for verifying reported anthropogenic natural gas usage. Here we present the development and initial results of a novel measurement system of atmospheric He that paves the way for establishing a global monitoring network in the future.

1 Introduction

The helium content of air ~~is increasing due to~~is a promising tracer for anthropogenic perturbation of the carbon cycle because He and CO_2 emissions are coupled in the use of natural gas on a global scale (Birner et al., 2021; Boucher et al., 2018a; Lupton and Evans, 2013; Oliver et al., 1984; Sano et al., 1989, 2010; Pierson-Wickmann et al., 2001; Lupton and Evans, 2004), ~~as~~ demonstrated recently by Birner et al. (Birner et al., 2022). The more abundant isotope of helium, 4-helium (^4He), is produced by the alpha decay of uranium and thorium-baring minerals in the subsurface and accumulates on geological timescales in the same underground reservoirs as natural gas. Natural gas extraction therefore also extracts He, which is released into the atmosphere during purification, storage, or ~~usage~~ burning of natural gas. Since other fossil fuels are thought to contain much

less helium than natural gas (Oliver et al., 1984; Pierson-Wickmann et al., 2001), helium may prove to be a valuable conservative tracer for the consumption of natural gas, which could aid efforts to quantify global emissions with top-down techniques.

Relying on archived air samples, Birner et al. (2022) used a new, highly-precise method for quantifying changes in the atmospheric Helium-to-nitrogen ratio (He/N_2) to show that the atmospheric concentration of ^4He increased by 1.930±0.140 per mille since 1974. Observed differences in He/N_2 (or He/M) between samples and an atmospheric air reference gas are reported here in units of per meg (1000 per meg = 1 per mille) using delta notation:

$$\delta(He/N_2)[per\ meg] = \left(\frac{\left(\frac{He}{N_2}\right)_{Sample}}{\left(\frac{He}{N_2}\right)_{Reference}} - 1 \right) \times 10^6 \quad (1)$$

The atmospheric build-up has accelerated over time, paralleling natural gas usage, yielding a rate of rise in 2020 of ~66 per meg per year, based on the published curve fit.

The measurements by Birner relied on a getting method which resolves small changes in the ~~"getter-helium" method pioneered by Birner et al. (Birner et al., 2021, 2022) developed a precise method for measuring changes in the atmospheric~~ measures ~~changes in the~~ ^4He mole fraction (He/M) of~~in~~ dry air by stabilizing the flow of an air sample and air-like reference gas to a continuously evacuated magnetic sector mass spectrometer (MS). By holding the air flow constant regardless of the gas source, changes in $^4He^+$ ion beam intensity reflect~~ed~~ changes in the helium mole fraction between the sample and reference. Directly upstream of the MS, the He ~~was~~ is concentrated by removing ("gettering") the non-noble gases using a hot titanium sponge. The observed changes in He/M are subsequently~~are then~~ converted to equivalent changes in ~~helium to nitrogen ratio (~~He/N_2~~)~~ by taking account of changes in the major components of air ~~using~~ constrained by separate observations of CO_2, O_2, and Ar (see section 2.6). The He preconcentration step is necessary to achieve strong He^+ beams and highest precision but precludes a direct measurement of He/N_2. However, ~~R~~reporting changes in terms of He/N_2 has the advantage that N_2 is present at near-constant levels in the atmosphere while denominator M – the total moles of dry air – may change from a variety of different processes that affect the overall composition of air (Keeling and Shertz, 1992; Keeling et al., 1998; Birner et al., 2022, 2021). ~~For~~ In any case, for most air samples the correction from He/M to He/N_2 is small~~, however,~~ because changes in CO_2 and O_2 partially cancel. ~~Observed differences in He/N_2 (or He/M) between samples and the reference gas are reported in units of per meg (1000 per meg = 1 per mille) using delta notation:~~

~~$$\delta(He/N_2)[per\ meg] = \left(\frac{\left(\frac{He}{N_2}\right)_{Sample}}{\left(\frac{He}{N_2}\right)_{Rerference}} - 1 \right) \times 10^6$$~~

~~Relying on archived air samples, Birner et al. (2022) used this "getter-helium" method to show that the atmospheric concentration of ^{4}He increased by 1930±140 per meg since 1974. The atmospheric build up has accelerated over time, paralleling natural gas usage, yielding a rate of rise in 2020 of ~ 66 per meg per year, based on the published curve fit.~~

Natural gas emissions must cause He/N_2 to vary on a wide range of space and time scales that remain to be resolved. For such applications, ~~Despite obtaining unprecedented precision,~~ the published "getter-helium" method has the limitation of requiring large air samples, substantial analysis time, and regular replacement of the getter material. This makes the method inconvenient for routine measurements of short-term changes in He/N_2 which are needed for tracing local pollution sources and evaluating air transport effects.

Here we present an alternative He measurement~~/N$_2$~~ method that uses a different pressure-stabilization/switching system and substitutes a cryogenic trap for the titanium sponge getter. This "cryo-enrichment" method avoids the flow corrections of Birner et al. (2021, 2022), improves precision, and allows automated and nearly continuous measurements, because the cryo-trap can be regenerated by a brief 25-minute warming cycle. We illustrate the method by detecting quasi-continuous He/N_2 variations over several weeks in air drawn from the pier of Scripps Institution of Oceanography ("Scripps Pier") in La Jolla, California, USA.

2 Method

2.1 Description of the gas delivery system

The gas delivery and purification components of the cryo-enrichment system for He analysis are illustrated in Figure 1. In the method, gas from an air intake and several reference gas cylinders is dried and routed through a Licor non-dispersive infrared CO_2 analyzer to our He detection system. The gas flow is precisely stabilized for rapid and robust sample-reference comparison before entry into a cryo-enrichment system (gray box in Fig. 1), where incondensable gases become concentrated in the gas stream in preparation of the helium mole fraction measurement on a dynamically-pumped magnetic sector mass-spectrometer (MS). The MS used for our experiments is a GV Isoprime 100, which is functionally comparable here to the MAT 253 used by Birner et al (2022) in previous He/M measurements.

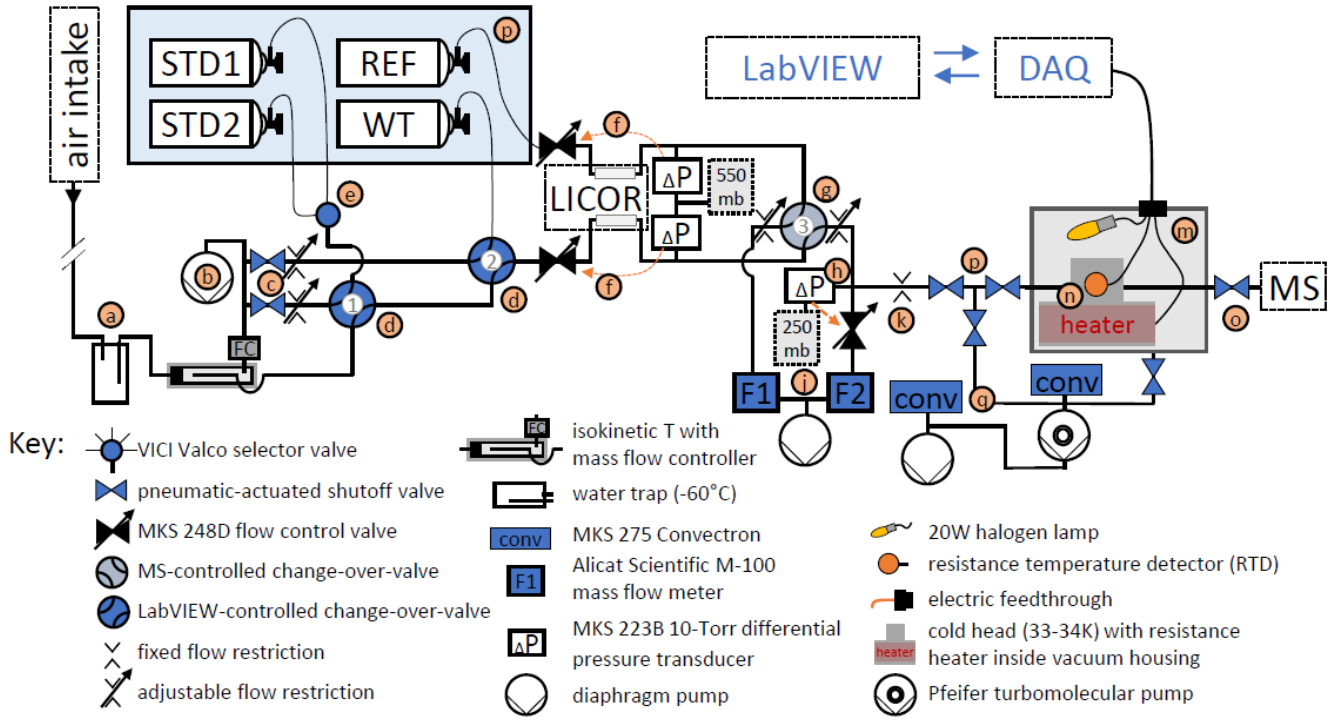

Figure 1. Schematic of gas delivery and purification for He/M measurements. Orange arrows indicate an analogue control loop using a MKS 250E flow control module. Letters highlight sections discussed in the text. All elements shown in blue face color are connected to a data acquisition system (DAQ) and controlled using LabVIEW software.

Gas is drawn through an aspirated intake (Blaine et al., 2006) located near the landward end of the Scripps Pier through ~250 m of ¼" Synflex tubing (i.e., "Pier Line II") to the lab facility at a flow of ~330 $cm^3\ min^{-1}$ STP and dried in a cold trap held at -60°C (a). In an isokinetic T, ~10% of the Pier Line II gas stream is split off for analysis while the rest flows metered at 300 $cm^3\ min^{-1}$ STP to a diaphragm pump (b), which also serves to pull the air from the pier through the main sampling line. Calibrated CO_2 span gases (e.g., STD1 & STD2), a working standard (WT), and the air-like instrument references gas (REF) are stored horizontally in a thermal enclosure (p). Gas for analysis is selected by a combination of a selector valve (e) and three pneumatically actuated change-over-valves (COV, d&g). Pneumatic shutoff valves and manually-adjustable flow restrictions (c) located downstream of COV-1&2 allow gases that are currently not selected for analysis to be purged at a set rate if desired. Regulators on the cylinders maintain a constant pressure of ~700hPa above ambient in the delivery lines of the calibration gases upstream of the flow-control valves (f) whereas the pressure in Pier Line II line drops modestly below ambient from the aspirated intake to the flow-control valves. Together with downstream differential pressure transducers, the two flow control valves (f) establish a constant pressure of ~550 hPa in the sample and reference gas line regardless of gas source where the air flows through a Licor LI-6251 non-dispersive infrared CO_2 analyzer. COV-3 (g) is responsible for rapid switching between sample and reference gas and is automatically triggered by the MS software, IonVantage, every 10 seconds. The air from one port of COV-3 is directed toward the mass spectrometer, while air from the other port is discarded.

Immediately downstream of the sampling and waste port of COV-3 (g) the pressure is reduced again across two manual flow restrictions. The restriction on the sampling port allows for a second pressure stabilization point (h) held at 250 hPa to very high precision using a back-pressure regulation scheme consisting of a flow-control valve in combination with a sensitive (10-torr) differential pressure gauge referenced to a static volume. From that stabilization point, ~0.3 STP cm^{-3} min^{-1} is picked off to flow towards the cryo-trap (m) at the inlet of the GV Isoprime 100 magnetic sector mass spectrometer (MS) while the rest is discarded to a second diaphragm vacuum pump. Flows through both outlets of COV-3 are carefully matched to a value of ~ 30 cm^3 min^{-1} STP by adjusting the manual flow restrictions using flow meters F1 and F2 (j) for diagnosis. The pick-off flow into the cryo-system (through crimp k) is measured by briefly stopping the pick-off flow (using valve p) and measuring changes on F2. Maintaining constant pressure at the 250-hPa stabilization point is critical to ensure constant flow of gas to the MS, regardless of the position of COV-3.

2.2 Cryo-trap

In the cryo-trap (m), air passes through a 0.005" thin-walled 1/8" O.D. stainless-steel tubing which is fit tightly into a T-shaped cold head (n), both housed inside a vacuum chamber. The tubing is cooled by the cold head (n) attached to a Sunpower Inc. GTLT cryocooler (not shown) to a temperature of 33-34K, which freezes out most of the N_2, O_2, Ar, CO_2 and other condensable trace gases in the air stream, thereby increasing the He mole fraction in the exit flow by several orders of magnitude compared to the inlet flow. The cryocooler is equipped with a proportional integral controller and an RTD, installed on the cold head (n), which maintain cryogenic temperatures to within less than ±0.015K. The trap is regenerated by temperature cycling to ~300K and pumping away the trapped gases while isolating the MS with a shutoff valve (o). To warm up, power is supplied to a heater combination consisting of a 180W polyimide coated resistance heater mounted inside the cold head and a 20W halogen lamp, while the cryocooler is turned off temporarily. The complete heating and cooldown sequence takes approximately 25 min and is fully automated. A set of three valves (p) isolate the gas purification system from the gas delivery system during regeneration but allows gas to be pumped away from the cryo-trap at all times while warming up to prevent critical overpressure. Pressure in the vacuum system is monitored using two Convectron sensors (q).

An optimum target temperature for the cryocooler was determined empirically by maximizing the $^4He^+$ beam strength. Operating at this optimum also very conveniently minimizes the sensitivity of the He ion beam to temperature fluctuations in the trap. We speculate that this maximum exists because a finite amount of N_2 increases the ionization efficiency of the He. Below the optimum temperature, N_2 levels are too low to achieve maximum ionization efficiency, while above the optimum, N_2 levels are too high to achieve maximum efficiency. The optimum temperature was found to be in the range of 33-34K. This optimum temperature, which is based on the cold-head temperature rather than the temperature of the 1/8" tubing, is likely slightly somewhat sensitive to the specific ion source filament and the thermal conductivity between the cold head and the 1/8" tubing.

There is an inherent engineering and design conflict between minimizing the flushing time of the trap section, which determines the fastest permissible frequency of sample-reference comparisons, and the total trap capacity. On the one hand, a larger trap

can hold more frozen gas before blocking the flow and thus allows longer operation periods before regenerating and/or higher gas flow and thus ion beam intensities, yielding better precision. On the other hand, a larger trap takes longer to flush completely, and thus needs longer dead times during sample-reference switching. In the end, we settled on 1/8" tubing which gave an acceptable dead time of 4 seconds for flushing out the trap section and allowed 80-100min of measurement time before regeneration. Further optimization of design choices in this realm are likely possible.

2.3 Gas composition reaching the MS

The gas mixture reaching the He-MS after purification in the cryo-trap consists mostly of N_2 but is greatly enriched in He, Ne, and H_2 relative to air (Fig. 3). Although the measured $^4He^+$ beam is still 1450 times smaller than the $^{28}N_2^+$ beam due to the residual vapor pressure of N_2 at ~33K, we estimate that the He/N_2 ratio is increased 1000- to 1500-fold, taking into account the ~10x lower ionization efficiency of He. The ratios of O_2/N_2 and Ar/N_2 are also considerably lower in the gas mixture reaching the MS than in air because Ar, O_2, and CO_2 are more readily frozen out of the gas stream than N_2. A fraction of all ions become doubly charged in the MS and molecular species may be broken up in the ion source. These ions are visible as interferences at lower mass to charge ratios (m/z), such as $^{28}N_2^{2+}$ and $^{14}N^+$ at m/z=14.

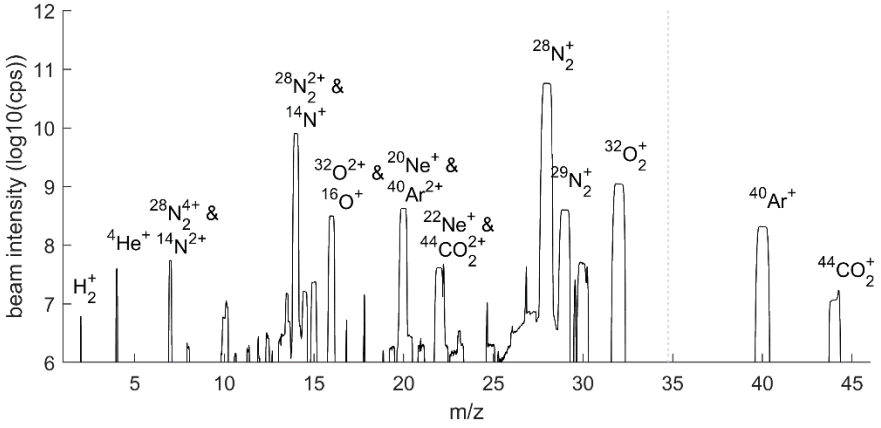

Figure 2. Mass Scan of gas mixture reaching the MS for helium analysis. Scans from two differently positioned Faraday cups are combined at the dashed vertical line to extend the region covered in the scan. Background concentrations of ions in the isolated MS have been removed. Unlabeled peaks are likely artifactual and the result of beam reflections or other beam aberrations in the flight tube.

2.4 CO_2 measurements and Calibration scheme

^{4}He/M and CO_2 were measured in parallel on the cryo-enrichment system, by comparing a sample gas stream against the instrument reference gas (REF, see Fig 1). In the "sample" stream, we analyzed air drawn either from Scripps Pier or from any of several calibration tanks containing compressed air at high pressure. To determine the long-term He/M stability of the cryo-enrichment system, a working tank (WT) was treated as an unknown and measured repeatedly over the course of the observation period, usually for 20 min every 2h. This caused the WT to be measured at different times in the regeneration and measurement cycle of the cryo-trap and on occasion caused the WT analysis to be missed when the timing coincided with the

regeneration cycle of the gas purification system. Calibrated high and low CO_2 span tanks (STD1 & STD2) were analyzed for 2x20 min each on one day roughly once a week to provide a two-point calibration for the CO_2 analyzer. Unfortunately, insufficient purging of stagnant gases in the pressure regulator and the delivery lines led to problems with the STD1-STD2 calibration and systematic differences of up to 0.15 ppm are evident between the first and second consecutive 20min measurement of these standards. Therefore, we consider CO_2 data measured on the cryo-enrichment system (i.e., Pier Line II) to only be calibrated to ±1 ppm, which is nevertheless sufficient to reliably resolve the large observed atmospheric changes in air drawn from the Scripps Pier. All CO2 data are reported in the SIO CO_2 scale X12. He/M data are reported in delta values (Eq. 1) relative to the instrument reference gas cylinder HA2373 which contains unpolluted air collected on 10th Feb. 2022.

2.5 ^{4}He/M data acquisition and corrections

~~All He/N_2 data are reported in delta values (Eq. 1) relative to the instrument reference gas. Pier Line II air data was averaged to 10 min where valid data was available for at least 1/3 of the 10 minute interval.~~

The scheduling of all data acquisition is controlled by LabVIEW which communicates with the IsoPrime MS using activeX controls. Every 10 minutes a new data acquisition is triggered by LabVIEW to maintain synchronization of the computer and MS internal clocks. Acquisitions consist of 58 regular switches between sample and reference gas each lasting a total of 20 seconds (10 sec sample & 10 sec reference). 4 seconds of data are discarded after each switch followed by 6 seconds of integration, taking into account a 1.8 sec delay between the switching event and the arrival of the switched gas at the MS.

Raw values provided by the MS and LabVIEW software environment need to be corrected for incomplete flush out during switching and the electronic baselines of the detector. This was done using two heuristic factors:

$$\delta\left({}^4He/M\right) = \left(1 - \frac{{}^4He^+_{BG}}{\overline{{}^4He^+}}\right)^{-1} \times \left(1 - 2 \times \frac{1}{6}\int_{t=4}^{t=10} \exp\left(-\frac{t}{1.4}\right) dt\right)^{-1} \times \delta\left({}^4He/M\right)_{raw} \quad (1)(2)$$

where raw delta values are defined as $\delta\left({}^4He/M\right)_{raw} \equiv \frac{2\times {}^4He^+_{SA}}{{}^4He^+_{-REF} + {}^4He^+_{+REF}} - 1$, ${}^4He^+_{SA}$ is the ion beam intensity of the sample averaged over a given 6-second integration window, and ${}^4He^+_{-REF}$ and ${}^4He^+_{+REF}$, are same for the reference gas in the windows before and after the given sample window. The electronic baseline or "background" signal ${}^4He^+_{BG} \approx 1$ nA is determined during periods when no gas is flowing into the MS and $\overline{{}^4He^+} \approx 9$ nA is the ^{4}He$^+$ beam measured when sample is entering the MS. The first factor in Eq. (2) accounts for the missing electronic baseline and has a magnitude of 112%. The second factor in Eq. (2) is close to 103% and corrects the raw delta values for a bias introduced by integrating data over 4 to 10 seconds after a switch between SA and REF gas while there is still residual drift in the ion beam from switching, which is characterized by an exponential with an e-folding scale of ~1.4 seconds.

To minimize artifacts associated with the transient response following changes between gases sources (e.g., air from the pier vs from a standard) or starting/stopping flow we discard data from certain periods in the measurement cycle. We reject all data points within: (i) 120 sec after restarting gas flow through the trap following a regeneration, (ii) 120 sec (180 sec for CO_2)

after switching between gas sources (e.g., WT, and Pier Line II air), and (iii) 120 sec after stopping gas flow to the MS for $^4He_{BG}$ determination. These times were chosen empirically from visible drift in the Licor and MS signals, respectively. In addition, the first delta value of each new MS acquisition is rejected as well as a small number of data points (~0.025%) for which the running standard deviation of the $^4He^+$ signal exceeded 8 fA, corresponding to over ten times the variability expected from ion counting statistics. Finally, Pier Line II air data is averaged to 10 min where valid data was available for at least 1/3 of the 10-minute interval.

2.6 Measurements of Ar, O_2, and CO_2 to derive δ(He/N_2) from δ(He/M)

To convert data from He/M into He/N_2, we use concurrent measurements of Ar/N_2, O_2/N_2, and the CO_2 mole fraction made routinely in the lab of R. Keeling at Scripps (see Fig. S1). These analyses are performed with a combination of a Licor Li-6251 CO_2 analyzer, a custom-built interferometric O_2 analyzer and a second GV IsoPrime 100 mass spectrometer for Ar/N_2 measurements which have been described in detail by Keeling et al. (Keeling et al., 2004, 1998). Like the cryo-enrichment system, these instruments are equipped with a ¼" gas delivery line drawing in air from Scripps Pier (i.e., "Pier Line I"). The gas delivery lines for the Ar, O_2 and CO_2 measurement system are separate from "Pier Line II", but the intake points are in close proximity and we find no systematic temporal offset between signals in both lines. This allows us to combine 10min-resolution observations from both sources as needed to calculate δ(He/N_2) from δ(He/M) according to Eq. (3) given by Birner et al. (2020):

$$\delta(He/N_2) \simeq \delta(He/M) + \delta(O_2/N_2)X_{O_2} + \delta(Ar/N_2)X_{Ar} + dX_{CO_2} \quad \text{~~(2)~~(3)}$$

where X_{O_2}=0.2095 and X_{Ar}=0.00934 are representative values of the atmospheric oxygen and argon mole fraction, and dX_{CO_2} are differences in the CO_2 mole fraction from a preindustrial value of 280 ppm. This correction averages -27.5 per meg and varies little over time with over 92% of all corrections falling within 20 per meg or less of the average correction. The O_2/N_2, Ar/N_2 and CO_2 corrections contribute negligible imprecision to the He/N_2 measurement based on their high precision relative to the measurement of He/M and because they are scaled down by factors X_{O_2} and X_{Ar}.

3 Results and discussion

3.1 Results for air measurements from the Scripps Pier

We used the newly-developed cryo-enrichment system and associated gas handling (Figure 1) to measure He/N_2 and CO_2 in air at Scripps Pier, La Jolla, intermittently over a 5-week period in April and May 2022, with 178 hours of total analysis time. He and CO_2 exhibit substantial diurnal and day-to-day variability (Fig. 3). He/M and He/N_2 vary by up to ~1500 per meg hour-to-hour and changes are tightly correlated with variability in CO_2 (Fig. 4). A linear model of their relationship yields a slope of ~20 per meg ppm^{-1} for He/M and CO_2 from Pier Line II, and of ~17 per meg ppm^{-1} for the combination of He/N_2 and CO_2 from Pier Line I. Differences in the CO_2 data from the two Licors measuring Pier Line I versus Pier Line II of several ppm

occur at times (Fig. 3). We speculate these differences may reflect impacts of very local emissions and small-scale transport features. This is supported by the stronger correlation between He and CO_2 data from the shared Pier Line II compared to the separate Pier Line I, suggesting the offsets reflect true atmospheric signals.

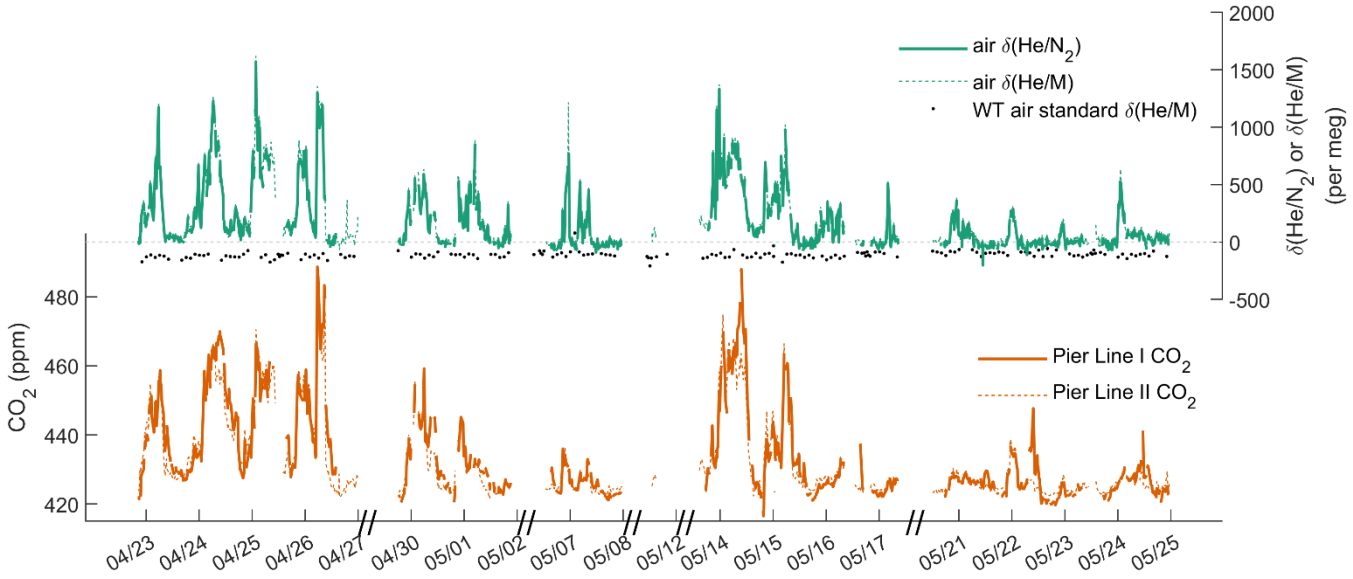

Figure 3. Time series of He/M, He/N_2, and CO_2 at Scripps Pier from Pier Line I and II. Repeat measurements of the WT standard offset by +100 per meg are shown to illustrate the stability of the system.

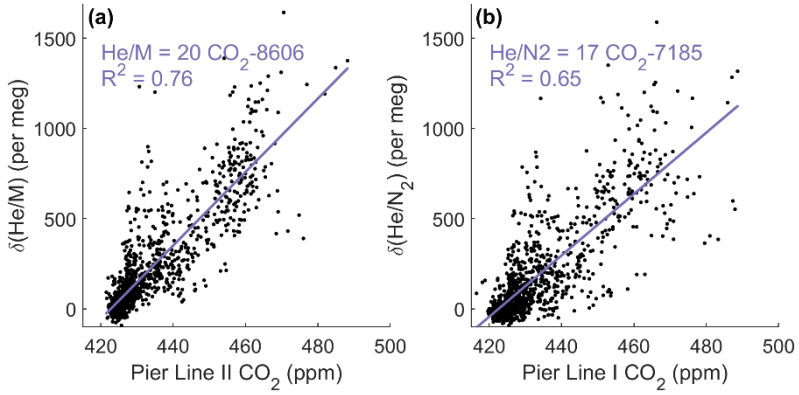

Figure 4. Correlation between (a) He/M and CO_2 from Pier Line II, and (b) He/N_2 and CO_2 from Pier Line I.

He and CO_2 at Scripps Pier are controlled by several influences, including local fossil fuel activity and atmospheric transport. Main local sources and sinks of CO_2 include gasoline, diesel, and natural gas emissions, as well as exchange of CO_2 with the local biosphere and soils. Contributions from these sources and sinks to the observed signals at Scripps Pier are modulated by local atmospheric transport. Although the high correlation of He and CO_2 signals suggest that local variability is dominated

by fossil fuel usage, as expected, there are a few episodes when the relationship between He and CO_2 deviates by more than 500 per meg from the fit line in Fig. 4, a decoupling of potential interest (if real) that warrants further investigation of local He and CO_2 sources. Air exchange with the He-rich stratosphere may also influence local tropospheric He levels while leaving CO_2 largely unaffected but these He signals are expected to be much smaller than the observed variations (Birner et al., 2021). The diurnal variations in CO_2 and He at Scripps Pier (Fig. 5) follow a land-breeze/sea-breeze pattern of local wind direction as previously seen in decades of quasi-continuous CO_2 measurements at costal sites in California (e.g., Manning et al., 1999; Riley et al., 2005). This diurnal cycle has an average max-min amplitude of 450-500 per meg in δ(He/M) over our specific observation period. During the day, enhanced vertical mixing and onshore winds bringing in relatively pollution-free marine boundary layer air, leading to lower He and CO_2 concentrations at Scripps Pier. At night the pattern reverses, with reduced vertical mixing and stronger influences from emission on land (fuel burning and respiration) increasing both CO_2 and He. Correspondingly, CO_2 and He/M vary substantially from day to day during the night and in the early morning whereas in the afternoon, CO_2 and He/M converge towards a more stable background level.

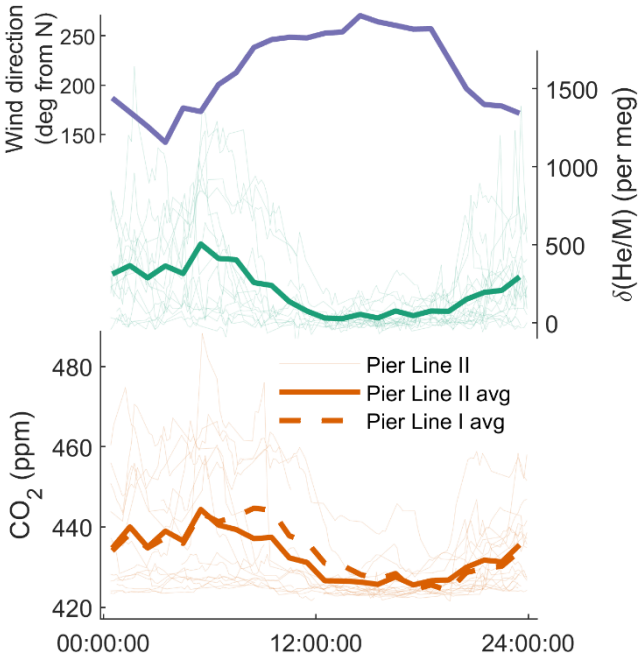

Figure 5. Diurnal cycle at Scripps Pier of prevailing wind direction, He/M, and CO_2 from the Pier Line I, or Pier Line II. (Vector) averages are computed from the time series shown in Fig. 3 and reported in Pacific Standard Time. Wind data for the same period is provided by Costal Data Information Program Station 073 available here https://cdip.ucsd.edu.

3.2 System stability

Repeat analyses of the working tank (WT) suggest the cryo-enrichment system for He analysis maintained good reproducibility over the 5-week period of the pier line measurements. Repeat comparisons of the WT against the instrument reference gas every 2-4 hours are show in Figs. 3 and 6. These measurements show little drift by eye, but a one-way ANOVA analysis

reveals significant ($p= 1.3x10^{-07}$) differences between measurements clustered by time into 5 groups. Average δ(He/M) values have standard deviation of ±10.5 per meg between groups. The origin of this variability remains unknown, but we speculate it may be caused by a small and variable thermal fractionation effect as gas is taken out of the high-pressure cylinders. To address this small drift regardless of origin, we apply a smooth spline to all WT data (see Fig. 6) which we use as a time-varying correction for all He/M observations. The standard deviation of all replicate WT measurements after removing this fit line is 18.6 per meg, and thus about 1.3 times greater than the 14.1 per meg variability expected from ion counting statistics alone. Based on the 1.3 ratio of WT repeatability to ion counting noise and an average of 24 valid data points contained in a 10 min interval, we estimate the average uncertainty of 10 min He/M and He/N_2 data to be ~22 per meg.

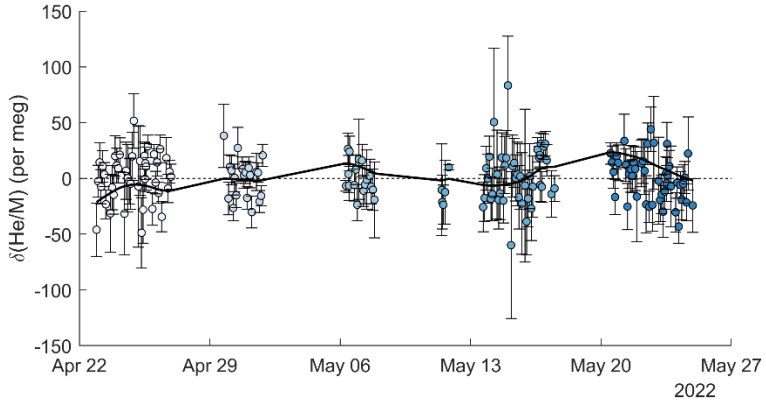

Figure 6. Repeat comparison of the working tank standard and the instrument reference gas. Error bars are calculated as the standard error of all standard-to-reference comparisons contributing to individual datapoints and differ in size mostly because some replicates consist of different number of comparisons. Marker face colors show the clustering into 5 groups used for ANOVA analysis (see text). A smooth spline is fit to the data and shown as a solid black line.

3.3 He in local emissions

Assuming the He/CO_2 ratios measured at Scripps Pier are characteristic of San Diego County, one can estimate the He abundance in local natural gas from our observed He/CO_2 ratio. Natural gas was on average responsible for 7.8 percent or 1.37 MtC of 19.01 MtC total carbon emissions in San Diego County between 2011 and 2015 (Gurney et al., 2020). Assuming an atmospheric He content of 5.24 ppm (Glückauf, 1944), the observed relationship between the He and CO_2 mole fraction of 20 per meg ppm^{-1}, can be alternatively expressed as 1.05×10^{-4} ppm He per ppm of CO_2. Taking into account the dilution of 1.37 MtC from natural gas emissions by 17.64 MtC from He-free fossil CO_2 emission sources (e.g., petroleum, etc), we estimate an average He content of natural gas used in San Diego of $1.05\times10^{-4}/0.078 = 0.13\%$ (mol He per mol CO_2). This is about 4 times greater than the global He content of natural gas reported by Birner et al. (Birner et al., 2022). Although a higher local He content is consistent with anomalously high He levels previously reported in US natural gas resources (Oliver et al., 1984), US natural gas production has largely transitioned to fracking with a potentially different helium signature since this estimate was made in 1984.

3.4 Implications of high-frequency variability for archived air samples

Birner et al. (2022) briefly discussed the possibility that some of the scatter seen in He/N_2 measurements of archived air from Scripps Pier may be the result of real in-situ variability and reflect varying levels of local pollution. Although our cryo-enrichment method indeed revealed hourly He/N_2 variability of over 1000 per meg at Scripps Pier, this variability likely did not substantially bias the archived air samples because they were generally filled under west-wind conditions to minimize local pollution influences. In addition, many of the samples were evaluated previously for several other tracers and yielded background values (Mühle et al., 2010). However, real atmospheric He/N_2 variability at the level of ~~several 10th of~~ ~50 per meg captured by the tanks cannot be excluded on the basis of these observations alone.

3.5 Future applications

The He/N_2 ratio is expected to feature rich variability on a wide range of spatial and temporal scales (Birner et al., 2021). We expect a seasonal cycle in the He mole fraction of unpolluted air caused by exchanges of N_2 and He with the ocean due to temperature-driven solubility changes. The seasonal cycle in polluted air in contrast should reflect seasonal changes in natural gas usage and large-scale changes in prevalent wind direction which modulate the influence of regional and national pollution sources. In addition, He/N_2 may vary interannually due to exchange of air with the stratosphere (Holton et al., 1995), where He is likely enriched compared to the troposphere by gravitational fractionation, which has been shown to deplete Ar/N_2 in the stratosphere (Birner et al., 2021, 2020; Ishidoya et al., 2013, 2008). The Quasi-Biennial Oscillation modulates the stratosphere-troposphere exchange and thus the interannual variability in the troposphere of several tracers including N_2O, CFCs and ^{14}C (e.g., Graven et al., 2012; Montzka et al., 2018; Nevison et al., 2011; Ray et al., 2020; Salby & Callaghan, 2006). A similar QBO signal is expected in the He mole fraction at locations with significant stratospheric influence such as La Jolla (Škerlak et al., 2014) although the magnitude of such a signal remains uncertain. Decadal to centennial variability of atmospheric He levels is controlled by anthropogenic fossil fuel usage. Based on a curve fit to He/N_2 measurements of archived air from 1974 to 2020, the global atmospheric He/N_2 ratio increased by ~66 per meg yr^{-1} in 2020 (Birner et al., 2022) which should emerge from the noise with only several months of observations at a one location, such as Scripps Pier, given sufficient stability of standard gases as supported by the good reproducibility of repeat measurements of a single standard cylinder shown here. We also expect spatial gradients in He because natural gas emissions are concentrated in the Northern Hemisphere, likely producing a clear interhemispheric difference. Spatial gradients may also occur on smaller scales related to human or geological emissions that so far have been too small to quantify well using other observational methods (Boucher et al., 2018b; Sano et al., 2010).

The cryo-enrichment method seems suitable, not just for continuous in situ measurements of He/N_2, but also for flask measurements, enabling the targeting of these spatial and temporal signals. The improved precision (22 per meg in 10 min) and small sample consumption (300 ml in 10 min) of the cryo-enrichment method enable interfacing with a setup for air sample flask analysis and/or establishing in-situ monitoring stations in different locations. In-situ and flask monitoring of atmospheric

He levels at local and global scales will also allow including He as a new tracer into atmospheric inversion frameworks where it may provide valuable information on carbon emissions sources by clearly attributing some fraction of emissions to natural gas usage. For this application to succeed, He characteristic of natural gas used must also be known, driving a need for future sampling of either pipeline gas directly or exhaust gas of power plants. Analysis of flasks from different sampling locations will provide a means to study spatial heterogeneity in atmospheric helium as well which has additional useful applications. For example, the magnitude of the interhemispheric gradient may inform our understanding of interhemispheric mixing, similar to previous studies using SF_6 (e.g., Patra et al., 2009).

3.6 Measuring H_2 and Ne

~~Finally, t~~The cryo-enrichment method may also be suitable for high-precision measurements of other ratios, including H_2/N_2, neon isotopes and He/Ne in atmospheric samples. H_2 levels in the atmosphere have increased over time and additional emissions are expected from a transition to hydrogen fuels (Patterson et al., 2021) but~~, ~~current H_2 analysis methods suffer from non-linearity in the detector response requiring sophisticated calibration schemes and typically achieve a moderate precision of roughly 1 per mille (Jordan and Steinberg, 2011). Atmospheric Ne has no large known sources or sinks and therefore no substantial spatial or temporal variability is expected in its isotopes but this has not been confirmed observationally due to a lack of sufficiently precise measurements. The He/Ne ratio should generally be controlled by variations in atmospheric He levels and mimic the behavior of He/N_2 but may provide additional information in the analysis of gas mixtures from some natural geological sources which can be enriched or depleted in N_2. Both H_2 and Ne are readily detectable on our system because both have sufficiently low boiling points to pass through our cryo-enrichment unit without getting trapped. Ion beams of H_2 and the two most common Ne isotopes are clearly distinguishable from the backgrounds in a mass scan (Fig. 2) suggesting a precision substantially below 100 per meg may be attainable. However, H_2 measurements are complicated by large and variable background levels in the instrument and ^{20}Ne and ^{22}Ne suffer from interferences of doubly charged ^{40}Ar and $^{44}CO_2$. Although adjusting the trap temperature and ion source setting may help reduce these artifacts, some correction will likely be needed. Assuming 1% of Ar and CO_2 ions become doubly charged in the MS, corrections would amount to 0.5% and 0.3% of the ^{20}Ne and ^{22}Ne beams respectively. This seems acceptable, given that the presence of Ar and CO_2 can be measured precisely and is primarily a function of trap temperature and thus not expected to vary substantially during sample-reference switching.

3.7 Conclusion

High-precision measurements of atmospheric helium levels in-situ and in sample flasks, enabled by the cryo-enrichment method presented here, have great potential to improve our understanding of the anthropogenic carbon cycle, to which helium is intimately connected through co-emission of He and CO_2. Validation experiments and semi-continuous measurements of He/M during local pollution events at Scripps Pier shown here, demonstrates that the new method further improves precision

and overcomes previous ease-of-use limitations of the "getter-helium" method employed by Birner et al. (Birner et al., 2022, 2021), thereby paving the way for establishing He as an important part of the trace gas toolkit in carbon cycle studies.

4 Data availability

All data ~~will be made~~are publicly available ~~via the Scripps O2 program website https://scrippso2.ucsd.edu/~~at the UC San Diego Library Digital Collections https://doi.org/10.6075/J0J966JF~~.~~

5 Competing Interests

The authors declare that they have no conflict of interest.

6 Author contributions

BB conceptualized, built, and tested the cryo-enrichment system in collaboration with EM and RK. BB developed the methodology and carried out the investigation. BB also performed all data curation and analysis and prepared the manuscript with contributions from all co-authors. This project was supervised by RK and primary funding for this work was provided through an NSF grant to RK co-prepared by BB and RK.

7 Acknowledgements

We thank Jeff Severinghaus, Jacob Morgan, Jessica Ng, Julia Dohner, Ross Beaudette, Bill Paplawsky, and Jennifer Seibel for insightful discussions and laboratory support in the development of the cryo-enrichment method. We also thank Bill Paplawsky, Jennifer Seibel, and Shane Clark for maintaining and operating the Ar/N_2, O_2/N_2 and CO_2 analysis systems in the Keeling laboratory. This work was supported by National Science Foundation grants AGS-1940361 and OPP-1922922 and by Eric and Wendy Schmidt via recommendation of the Schmidt Futures program. A patent application (US 63,393,478) describing the cryogenic gas purification system was filed on July 29, 2022, and contains further analytical advances that allow truly continuous He measurements.

6 References

Birner, B., Chipperfield, M. P., Morgan, E. J., Stephens, B. B., Linz, M., Feng, W., Wilson, C., Bent, J. D., Wofsy, S. C., Severinghaus, J., and Keeling, R. F.: Gravitational separation of Ar/N2 and age of air in the lowermost stratosphere in airborne observations and a chemical transport model, Atmos. Chem. Phys., 20, 12391–12408, https://doi.org/10.5194/acp-20-12391-

2020, 2020.

Birner, B., Paplawsky, W., Severinghaus, J., and Keeling, R. F.: Measurements of atmospheric He/N2 as an indicator of fossil fuel extraction and stratospheric circulation, Atmos. Meas. Tech., 14, 2515–2527, https://doi.org/10.5194/amt-14-2515-2021, 2021.

Birner, B., Severinghaus, J., Paplawsky, B., and Keeling, R. F.: Increasing atmospheric helium due to fossil fuel exploitation, Nat. Geosci., 15, 346–348, https://doi.org/10.1038/s41561-022-00932-3, 2022.

Blaine, T. W., Keeling, R. F., and Paplawsky, W. J.: An improved inlet for precisely measuring the atmospheric Ar/N_2 ratio, Atmos. Chem. Phys., 6, 1181–1184, https://doi.org/10.5194/acp-6-1181-2006, 2006.

Boucher, C., Marty, B., Zimmermann, L., and Langenfelds, R.: Atmospheric helium isotopic ratio from 1910 to 2016 recorded in stainless steel containers, Geochemical Perspect. Lett., 6, 23–27, https://doi.org/10.7185/geochemlet.1804, 2018a.

Boucher, C., Lan, T., Mabry, J., Bekaert, D. V., Burnard, P. G., and Marty, B.: Spatial analysis of the atmospheric helium isotopic composition: Geochemical and environmental implications, Geochim. Cosmochim. Acta, 237, 120–130, https://doi.org/10.1016/j.gca.2018.06.010, 2018b.

Glückauf, E.: A simple analysis of the helium content of air, Trans. Faraday Soc., 44, 436–439, 1944.

Graven, H. D., Guilderson, T. P., and Keeling, R. F.: Observations of radiocarbon in CO_2 at La Jolla, California, USA 1992-2007: Analysis of the long-term trend, J. Geophys. Res. Atmos., 117, 1–14, https://doi.org/10.1029/2011JD016533, 2012.

Gurney, K. R., Liang, J., Patarasuk, R., Song, Y., Huang, J., and Roest, G.: The Vulcan Version 3.0 High-Resolution Fossil Fuel CO2 Emissions for the United States, J. Geophys. Res. Atmos., 125, 1–27, https://doi.org/10.1029/2020JD032974, 2020.

Holton, J. R., Haynes, P. H., Mcintyre, M. E., Douglass, A. R., and Rood, B.: Stratosphere-Troposphere exchange, Rev. Geophys., 33, 403–439, 1995.

Ishidoya, S., Sugawara, S., Morimoto, S., Aoki, S., and Nakazawa, T.: Gravitational separation of major atmospheric components of nitrogen and oxygen in the stratosphere, Geophys. Res. Lett., 35, 1–5, https://doi.org/10.1029/2007GL030456, 2008.

Ishidoya, S., Sugawara, S., Morimoto, S., Aoki, S., Nakazawa, T., Honda, H., and Murayama, S.: Gravitational separation in the stratosphere - A new indicator of atmospheric circulation, Atmos. Chem. Phys., 13, 8787–8796, https://doi.org/10.5194/acp-13-8787-2013, 2013.

Jordan, A. and Steinberg, B.: Calibration of atmospheric hydrogen measurements, Atmos. Meas. Tech., 4, 509–521, https://doi.org/10.5194/amt-4-509-2011, 2011.

Keeling, R. and Shertz, S.: Atmospheric oxygen and implications for the global carbon cycle, Nature, 358, 723–727, https://doi.org/10.1038/358723a0, 1992.

Keeling, R. F., Manning, A. C., McEvoy, E. M., and Shertz, S. R.: Methods for measuring changes in atmospheric O_2 concentration and their application in southern hemisphere air, J. Geophys. Res., 103, 3381–3397, https://doi.org/10.1029/97JD02537, 1998.

Keeling, R. F., Blaine, T., Paplawsky, B., Katz, L., Atwood, C., and Brockwell, T.: Measurement of changes in atmospheric

Ar/N_2 ratio using a rapid-switching, single-capillary mass spectrometer system, Tellus, 56B, 322–338, https://doi.org/10.1111/j.1600-0889.2004.00117.x, 2004.

Lupton, J. and Evans, L.: The atmospheric helium isotope ratio: Is it changing?, Geophys. Res. Lett., 31, 1–4, https://doi.org/10.1029/2004GL020041, 2004.

Lupton, J. and Evans, L.: Changes in the atmospheric helium isotope ratio over the past 40 years, Geophys. Res. Lett., 40, 6271–6275, https://doi.org/10.1002/2013GL057681, 2013.

Manning, A. C., Keeling, R. F., and Severinghaus, P.: Precise atmospheric oxygen measurements with a paramagnetic oxygen analyzer several repeated measurements interval various aspects of the global The analyzer was used to measure atmospheric period strongly changes sources to define, Global Biogeochem. Cycles, 13, 1107–1115, 1999.

Montzka, S. A., Dutton, G. S., Yu, P., Ray, E., Portmann, R. W., Daniel, J. S., Kuijpers, L., Hall, B. D., Mondeel, D., Siso, C., Nance, J. D., Rigby, M., Manning, A. J., Hu, L., Moore, F., Miller, B. R., and Elkins, J. W.: An unexpected and persistent increase in global emissions of ozone-depleting CFC-11, Nature, 557, 413–417, https://doi.org/10.1038/s41586-018-0106-2, 2018.

Mühle, J., Ganesan, A. L., Miller, B. R., Salameh, P. K., Harth, C. M., Greally, B. R., Rigby, M., Porter, L. W., Steele, L. P., Trudinger, C. M., Krummel, P. B., O'Doherty, S., Fraser, P. J., Simmonds, P. G., Prinn, R. G., and Weiss, R. F.: Perfluorocarbons in the global atmosphere: Tetrafluoromethane, hexafluoroethane, and octafluoropropane, Atmos. Chem. Phys., 10, 5145–5164, https://doi.org/10.5194/acp-10-5145-2010, 2010.

Nevison, C. D., Dlugokencky, E., Dutton, G., Elkins, J. W., Fraser, P., Hall, B., Krummel, P. B., Langenfelds, R. L., O'Doherty, S., Prinn, R. G., Steele, L. P., and Weiss, R. F.: Exploring causes of interannual variability in the seasonal cycles of tropospheric nitrous oxide, Atmos. Chem. Phys., 11, 3713–3730, https://doi.org/10.5194/acp-11-3713-2011, 2011.

Oliver, B. M., Bradley, J. G., and Farrar IV, H.: Helium concentration in the Earth's lower atmosphere, Geochim. Cosmochim. Acta, 48, 1759–1767, https://doi.org/10.1016/0016-7037(84)90030-9, 1984.

Patra, P. K., Takigawa, M., Dutton, G. S., Uhse, K., Ishijima, K., Lintner, B. R., Miyazaki, K., and Elkins, J. W.: Transport mechanisms for synoptic, seasonal and interannual SF6 variations and "age" of air in troposphere, Atmos. Chem. Phys., 9, 1209–1225, https://doi.org/10.5194/acp-9-1209-2009, 2009.

Patterson, J. D., Aydin, M., Crotwell, A. M., Pétron, G., Severinghaus, J. P., Krummel, P. B., Langenfelds, R. L., and Saltzman, E. S.: H2 in Antarctic firn air: Atmospheric reconstructions and implications for anthropogenic emissions, Proc. Natl. Acad. Sci. U. S. A., 118, 1–8, https://doi.org/10.1073/pnas.2103335118, 2021.

Pierson-Wickmann, A. C., Marty, B., and Ploquin, A.: Helium trapped in historical slags: A search for temporal variation of the He isotopic composition of air, Earth Planet. Sci. Lett., 194, 165–175, https://doi.org/10.1016/S0012-821X(01)00554-4, 2001.

Ray, E. A., Portmann, R. W., Yu, P., Daniel, J., Montzka, S. A., Dutton, G. S., Hall, B. D., Moore, F. L., and Rosenlof, K. H.: The influence of the stratospheric Quasi-Biennial Oscillation on trace gas levels at the Earth's surface, Nat. Geosci., 13, 22–27, https://doi.org/10.1038/s41561-019-0507-3, 2020.

Riley, W. J., Randerson, J. T., Foster, P. N., and Lueker, T. J.: Influence of terrestrial ecosystems and topography on coastal CO 2 measurements: A case study at Trinidad Head, California, J. Geophys. Res., 110, 1–15, https://doi.org/10.1029/2004jg000007, 2005.

Salby, M. L. and Callaghan, P. F.: Influence of the Brewer-Dobson circulation on stratosphere-troposphere exchange, J. Geophys. Res. Atmos., 111, 1–9, https://doi.org/10.1029/2006JD007051, 2006.

Sano, Y., Wakita, H., Makide, Y., and Tominaga, T.: A ten-year decrease in the atmospheric helium isotope ratio possibly caused by human activity, Geophys. Res. Lett., 16, 1371–1374, https://doi.org/10.1029/GL016i012p01371, 1989.

Sano, Y., Furukawa, Y., and Takahata, N.: Atmospheric helium isotope ratio: Possible temporal and spatial variations, Geochim. Cosmochim. Acta, 74, 4893–4901, https://doi.org/10.1016/j.gca.2010.06.003, 2010.

Škerlak, B., Sprenger, M., and Wernli, H.: A global climatology of stratosphere-troposphere exchange using the ERA-Interim data set from 1979 to 2011, Atmos. Chem. Phys., 14, 913–937, https://doi.org/10.5194/acp-14-913-2014, 2014.